ECMWF Atmospheric Profiles in Maroua, Cameroon: Analysis and Overview of the Simulation of Downward Global Solar Radiation

Cyrille Fotsing Talla [1,2,*] iD, Donatien Njomo [1] iD, Céline Cornet [3], Philippe Dubuisson [3] and Leonard Akana Nguimdo [1,4]

[1] Environmental Energy Technologies Laboratory (EETL), Department of Physics, University of Yaounde 1, P.O. Box 812, Yaounde, Cameroon; dnjomo@usa.net (D.N.); languimdo@yahoo.fr (L.A.N.)
[2] Department of Physics, Higher Teachers' Training College, University of Maroua, P.O. Box 55, Maroua, Cameroon
[3] Univ. Lille, CNRS, UMR 8518–LOA–Laboratoire d'Optique Atmosphérique, F–59000 Lille, France; celine.cornet@univ-lille1.fr (C.C.); philippe.dubuisson@univ-lille1.fr (P.D.)
[4] Department of Electrical and Electronic Engineering, Faculty of Engineering and Technology, University of Buea, P.O. Box 63, Buea, Cameroon
[*] Correspondence: tallacyrille@yahoo.fr; Tel.: +237-677-341-172

Abstract: Atmospheric analysis data from the European Center for Medium-Range Weather Forecasts (ECMWF) have been acquired and are used to characterize the meteorological situation in Maroua, Cameroon (10.614° N, 14.361° E) at 12:00 UTC. These are then used to simulate downward global solar radiation (DGSR) with the moderate-resolution transmittance (MODTRAN) radiative transfer code (RTC). In comparison with meteorological data measured during the year 2014 in Maroua, ECMWF atmospheric quantities at ground level, in general, showed good correlation coefficients and slight differences. It is shown that ECMWF atmospheric profiles can thus be used to complete the scarce atmospheric data and to study the atmosphere state and dynamics, such as the African monsoon phenomenon detected in this region, which regulates the rainy season. In addition, they are more suitable to simulate clear-sky DGSR compared to MODTRAN standard atmospheric profiles. The causes and effects of the substantial bias and weak correlation coefficient observed with ECMWF wind data and the constant underestimation of simulated DGSR in comparison with ground-based measurements are investigated. The paper emphasizes the need for a better characterization of the Maroua atmosphere state and dynamics as well as the simulation of more accurate and reliable DGSR under any atmospheric conditions.

Keywords: ECMWF atmospheric profiles; meteorological data; African monsoon; solar radiation; MODTRAN

1. Introduction

The acquisition of atmospheric profiles and solar radiation data is a great challenge for developing countries such as Cameroon. These parameters play an important role in climate monitoring, environmental control and human activities [1,2], and they can be obtained through measurement, remotesensing or simulation [3]. In Maroua (10.614° N, 14.361° E), a locality situated in the far-north region of Cameroon, the meteorological situation is not well known. There is no recent and continuing measurement, neither of diffuse, direct or global solar radiation, nor of atmospheric parameter and constituent profiles. Not only are meteorological dataset profiles hardly accessible, but the existing sunshine databases also present substantial disparities and contain some gaps [4]. The region is facing some climatic disturbances that cause flood disasters and perturbations in farming practices and

varieties sown [5]. Consequently, the living conditions of the population, farmers in particular, are seriously degraded as a result of these new weather conditions that may be induced by changes in the general atmosphere dynamics in this region [6,7].

In fact, Maroua is situated 10° N in West Africa, where the phenomenon of monsoon has been intensively studied during the African Monsoon Multidisciplinary Analysis (AMMA) project [8–11]. This occurs generally from May to September (Monsoon onset: May 15–June 30; peak monsoon July 1–August 14; late monsoon: August 15–September 15) with important disparities [8,10]. As shown in Figure 1, in West Africa, the atmospheric circulation is driven by the wet monsoon flux, coming from the southwest of the Guinea Gulf, and the warm and dry Harmattan flux, blowing south-westward from the desert [9]. During the winter, the wind blows from the cooler continent to the warmer ocean, and the atmosphere is generally dry. During the spring, the sun elevation warms up the surface; the continent is becoming warmer more rapidly than the ocean. The thermal contrast leads to a surface pressure gradient between the ocean with high pressure and the continent with low pressure that reinforces the Southern Hemisphere trade wind. The monsoon flux is then able to cross the Equator, bringing a large amount of humidity that favors the cloud convection and the rain. This convergence area near the surface, called the intertropical front (ITF), is positioned at about 20° N in summer and 5° N in winter. Higher in the atmosphere, the African easterly jet (AEJ) situated in the middle of the troposphere (between 4 and 6 km), moves the convergence zone, called the intertropical convergence zone (ITCZ), to the south.
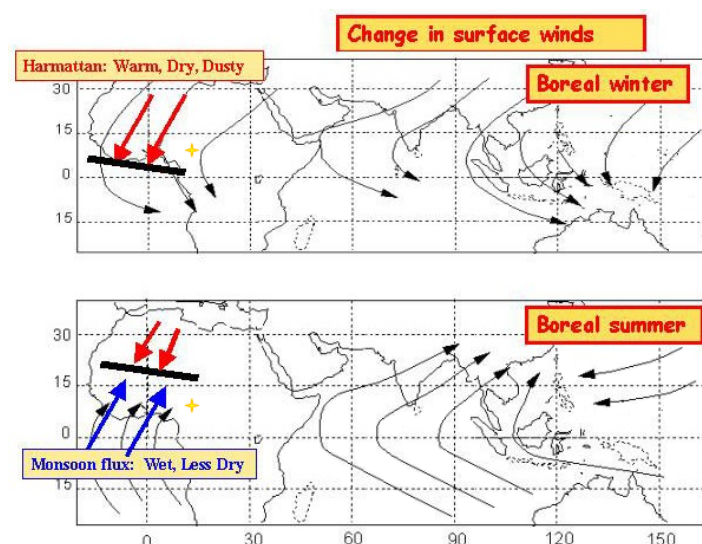

Figure 1. Schematic picture of the seasonal meteorological circulations in West Africa from http://www.amma-international.org/spip.php?article10. The yellow stars indicate the geographical position of Maroua.

Given that meteorological data in Maroua are most often measured only at ground level, efforts have to be made to acquire more atmospheric profiles and solar radiation data, in order to complete rare existing in situ measurements.

For the year 1984, aerosol thickness, cloud fraction profiles and water content were deduced from ground-level diffuse and global solar radiation measurements [12,13]. Unfortunately, this method could not be applied after 1984, as a result of the suspension of regular and reliable measurements, leading to an absence of a local recent database of diffuse and global solar radiation [4]. Nowadays, given that the atmosphere sounding with weather balloons is no longer available in Maroua, endowment with appropriate meteorological equipment is considered, but a certain time will be necessary to constitute good database series. Thus, currently, the easiest way to obtain access to atmospheric data may be by consulting global atmospheric databases such as standard atmospheric profiles, and real- or

near-real-time atmospheric data. These certainly have some limitations, but their usage may make the computation of solar data more realistic and even more accurate [14,15]. Dedicated centers, such as the European Center for Medium-Range Weather Forecasting (ECMWF), the National Aeronautics and Space Administration (NASA), and the National Oceanic and Atmospheric Administration (NOAA), collect and provide data for climate studies, weather forecasting or other purposes. Some, such as ECMWF, have Maroua in their observational data coverage, but as far as we know, no study on the validation of these data has been carried out in zone. We chose to use ECMWF databases that have been tried and tested elsewhere [16–19].

Maroua is located in an area of high solar potential, which can be exploited to overcome the local energetic and economic needs [20,21]. However, the control and exploitation of this solar energy require good updated knowledge of site's sunshine [22–24]. The Heliosat_2 method is used to derive global solar radiation from Meteosat satellite images [25]. It has been exploited to retrieve global daily solar irradiation in Cameroon but was established to be appropriate in Maroua only for monthly variations [26]. This method is under improvement to take into consideration surface albedo and vertical profiles and also to provide direct and diffuse irradiation as well as their spectral distribution [27,28]. Solar radiation can also be retrieved with good agreement using a parameterized solar radiative transfer model "CLIRAD-SW" radiative transfer code (RTC) and assuming a molecular atmosphere [29]. For a real situation, this approach can still be taken if an appropriate model of the atmosphere is used. This task requires robustness and flexibility of the RTC in the adjustment of parameters, and the moderate-resolution transmittance (MODTRAN) RTC is largely used for this purpose [30–34]. In addition, ECMWF global radiation data were validated against ground-based and regional model simulations [35,36], meaning that it may also be possible to reproduce this experiment in this region.

In summary, Maroua ground-level measurements should be consolidated and completed with data of upper atmospheric levels, in order to fully characterize the state of its atmosphere. This task must be reproducible over time in order to continuously provide meteorological observations and analyses as required for environmental purposes. Therefore, the present work shows the advantages of using relative recent measurements and accessible databases to fill the measurements gaps in Maroua. This study presents a method for permanent access to atmospheric parameters through the extraction of ECMWF vertical atmospheric profiles and their analysis. It also describes the simulation of solar radiation components with the MODTRAN RTC in the standard atmosphere. The impact of the insertion of ECMWF vertical profiles in simulations is finally evaluated by comparing simulated downward global solar radiation (DGSR), in clear-sky and various aerosol conditions, with in situ measurements.

2. Data and Methods

In this section, we present the data acquired to characterize the Maroua atmosphere and the process to use these as the input of the MODTRAN RTC.

2.1. ECMWF Atmospheric Profiles of 12:00 UTC

ECMWF routinely produces global analyses for the four main synoptic times 00, 06, 12 and 18 UTC and global 10 day forecasts on the basis of 12:00 UTC data [37,38]. We are interested in the ECMWF analysis database made up of observations that can roughly be divided into conventional (in situ) and non-conventional (remotesensing) observations. The ICARE Data and Services Center of the University of Lille 1 Science and Technology (http://www.icare.univ-lille1.fr) provided a set of ECMWF analysis data of 12:00 UTC over Cameroon for the year 2014. These data are given on a 0.5° × 0.5° grid and include the following:

- At the surface level: surface pressure (Sp), total column water vapor (TCWV), total column ozone (TCO) and total cloud cover (TCC).
- For 25 pressure levels, datasets of geopotential (ϕ), air pressure (P), air temperature (T), relative humidity (H) and horizontal wind components (U and V).

From this database, the Maroua site surface and atmospheric parameters were selected, and related parameters such as the height (Z) and horizontal wind speed (Va) were computed.

2.2. Measured Meteorological Data

In 2014, ground-level meteorological data were measured daily in Maroua (10.614° N, 14.361° E; 398 m) [4]. The Integrated Sensor Suite (ISS), the UV sensor and the solar radiation sensor of the Davis Vantage Pro2Plus weather station [39] were used in that experiment. Data collected during the campaign were the wind speed and direction, the atmospheric pressure, the temperature, humidity, and global UV radiation in the spectral range (290–390 nm), and the global solar radiation in the spectral range (300–1100 nm). These were archived with three temporal resolutions: 30 min from January to August, 5 min for September and 1 min from October to December. We note that the DGSR values are averaged on each archive interval. Referring to the available 12:00 UTC ECMWF atmospheric profiles, 12:00 UTC meteorological data of this campaign were extracted to constitute an annual meteorological measurement database that will be used for further comparison.

2.3. MODTRAN Radiance Simulation with Standard and ECMWF Atmospheric Profiles

This subsection is a brief presentation of some features of the RTC MODTRAN4 Version 1 Revision 1 used for the simulations. One can refer to the user manual [40] or MODTRAN report [41] for more explicit explanations.

MODTRAN code is one of the state-of-art radiative transfer computer codes. It integrates over the radiance contribution of a finite number of homogeneous layers in order to obtain the transmittance or radiance for a specified atmosphere. The band model parameters are generated from the high-resolution transmission molecular absorption database HITRAN96 [42,43], and the code has a set of standard atmospheric profiles.

The inputs of each MODTRAN simulation stand on one single input file (file_name.tp5) constituted of at least five CARDs. A CARD is a line of up to 80 characters using a fixed-format input. This file enables the user to choose among six geographical–seasonal standard atmosphere models, derived from 1986 Air Force Geophysics Laboratory (AFGL) atmospheric constituent profiles, or to specify a user-defined meteorological or radiosonde data profile (MODEL = 7). According to the Maroua geographical situation, we chose the "Tropical Atmosphere" profile (MODEL = 1) for the standard simulations. The total amount or vertical distribution of atmospheric constituents in this case was fixed to their default values. The parameter IHAZE identifies the aerosol model type used for the boundary layer (0–2 km) and default visibility (VIS). Table 1 presents the default aerosol models that could be used at the site of Maroua, considering its geographical situation. The new model IHAZE = 5bis with VIS = 23 km, derived from the model IHAZE = 5, has been added for comparison purposes. A wide range of cloud types, or none, can also be inserted into the atmosphere modeling. Simulations were made in the spectral range (300–1100 nm) with a resolution of 1 nm. Downward normal direct and diffuse solar radiation returned by MODTRAN were finally summed to calculate the DGSR.

Table 1. Description of MODTRAN default aerosol models that can be used in the site of Maroua. IHAZE is the aerosol model identifier and VIS represents the visibility.

IHAZE	Description
0	No aerosol or cloud attenuation included in the calculation
1	RURAL extinction; default VIS = 23 km
2	RURAL extinction; default VIS = 5 km
5bis	URBAN extinction; default VIS = 23 km
5	URBAN extinction; default VIS = 5 km
10	DESERT extinction; sets visibility from wind speed

Setting MODEL = 7 in MODTRAN allowed for some adjustments to the previous standard atmosphere, permitting the introduction of ECMWF atmospheric profiles. TCWV and TCO amounts were inserted into CARD 1A, while wind speed data were introduced into CARD 2. At each ECMWF level altitude, the corresponding P, T and H values were inserted, and the remaining level variables were defaulted to tropical standard atmosphere values. These insertions were made into CARDs 2C, 2C1 and 2C2.

3. Results and Analysis

3.1. Comparison of ECMWF and Measured Meteorological Data at Ground Level

In order to simulate radiances with ECMWF atmospheric profiles, we checked the consistency of the ECMWF data used as inputs to the measurements carried out at the site. For ground level, this is presented in Figure 2 through the comparison of the pressure, temperature, humidity and wind speed in Maroua in 2014. The corresponding annual averages, correlation coefficients (R), root-mean-squared errors (RMSEs) and mean bias errors (MBEs) are summarized in Table 2. Surface pressures correlated very well (R = 0.966). Despite that ECMWF data slightly underestimated low pressure and overestimated high pressure, error was weak. For the temperature, the correlation was also good (R = 0.894), and ECMWF data slightly underestimated the measurements (MBE = −1.6 °C). The RMSE of estimation was also small. Concerning humidity, the correlation was good again (R = 0.948). ECMWF data were slightly greater than measurements with an increasing error for high humidity. We note that this may also slightly have accentuated errors in the DGSR, as humidity is highly related to water vapor, which is a great modulator of solar radiation. The correlation coefficient for the wind speed was, on the contrary, weak. In numerical weather prediction (NWP) models such as ECMWF, turbulent diffusion under stable conditions is artificially enhanced to improve the representation of near-surface temperatures and synoptic cyclones [44]. This practice, which has often been used for tuning the large-scale performance of operational NWP models, is widely recognized to be detrimental for an accurate representation of stable atmospheric boundary layers [44–46]. Thus, it is not surprising that ECMWF data are greater than measurements, but the substantial biases observed and the way measured wind data appear, as shown in Figure 2c, bring us to suspect a problem with the anemometer used. These differences between ECMWF and measured winds at the surface led us to be very cautious with the results obtained for IHAZE = 10, as the wind surface is used to characterize desert dust uploading and visibility. Consequently, a comparison with other wind databases such as MERRA (https://gmao.gsfc.nasa.gov/reanalysis/MERRA/) or CFS (https://rda.ucar.edu/datasets/ds094.0/) is required to conclude on the accuracy of each source.

Apart from the wind speed, the ECMWF meteorological parameters at ground level are comparable to measurements, given the close annual averages, good correlation coefficients, and slight RMSE and MBE (Table 2). Additionally, the regression slopes indicated in Figure 2 are close to unity.

Table 2. Annual averages, correlation coefficient (R), Root-mean-squared error (RMSE), and mean bias error (MBE) of the site measured pressure (P), temperature (T), humidity (H) and wind speed (Va) in comparison with ground meteorological parameters extracted from European Center for Medium-Range Weather Forecasts (ECMWF) data in Maroua in 2014.

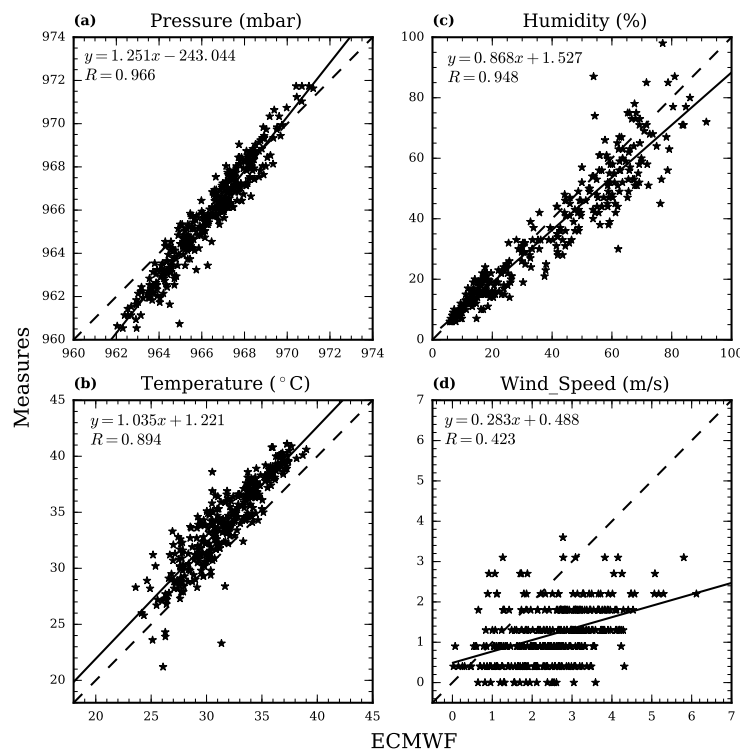| ECMWF vs Measures	Measures Annual Average	ECMWF Annual Average	R	RMSE	MBE
P (mbar)	966.553	966.290	0.953	0.868	−0.264
T (°C)	33.2	31.6	0.878	2.4	−1.6
H (%)	35.0	36.4	0.952	7.2	1.3
Va (m/s)	1.3	2.5	0.428	1.6	1.2

Figure 2. Comparison between meteorological parameters measured and those extracted from European Center for Medium-Range Weather Forecasts (ECMWF) data in Maroua in 2014 for (**a**) pressure, (**b**) temperature, (**c**) humidity and (**d**) wind speed at ground level. Solid lines represent linear regression curves and dashed lines are slope unity.

3.2. ECMWF Atmospheric Profiles

3.2.1. Total Column Quantities

To characterize atmospheric conditions at the Maroua site, the surface pressure and total column quantities for water vapor, ozone and cloud cover were extracted from the 2014 ECMWF database. The annual variations of these quantities are illustrated in Figure 3, where horizontal segments represent monthly averages. The TCC is particularly analyzed in Section 3.2.2.

Surface pressure is closely related to the atmospheric circulation described previously. During the first dry period, the surface pressure decreased from 967.2 mbar in January to the minimum value, about 964.0 mbar in April, when the monsoon flux takes place. Next, the pressure increased to reach a stable level around the maximum (968.2 mbar) between June and September in the wet period. Afterward, a slight decrease occurred during October and November, when the monsoon flux withdraws. The variation in the surface pressure in Maroua followed closely the variation presented in [47] at 10° N latitude with an annual average of 966.3 mbar. The regional circulation under the monsoon flux and the displacement of the ITCZ from South to North explain these variations and lead to the rainy season being between June and September in Maroua.

Regarding the TCWV average (32 kg/m^2) in 2014, a dry period (November–April) and a humid period (May–October) with potential rainfall appeared clearly. In January and February, the atmosphere was influenced by the dry Harmattan wind with TCWV values of around 14 kg/m^2. It gradually gained water vapor under the monsoon to reach a maximum of around 50 kg/m^2 from June to September. From the beginning of October, the content in the water vapor decreased gradually to 15 kg/m^2 in December with the return of the Harmattan. The variations and values of the TCWV in Maroua (10.61° N, 14.36° E; 398 m) that year were in the same order of magnitude as those measured by a microwave radiometric profiler in Niamey (13.48° N, 2.17° E; 223 m) during the year 2006 [11].
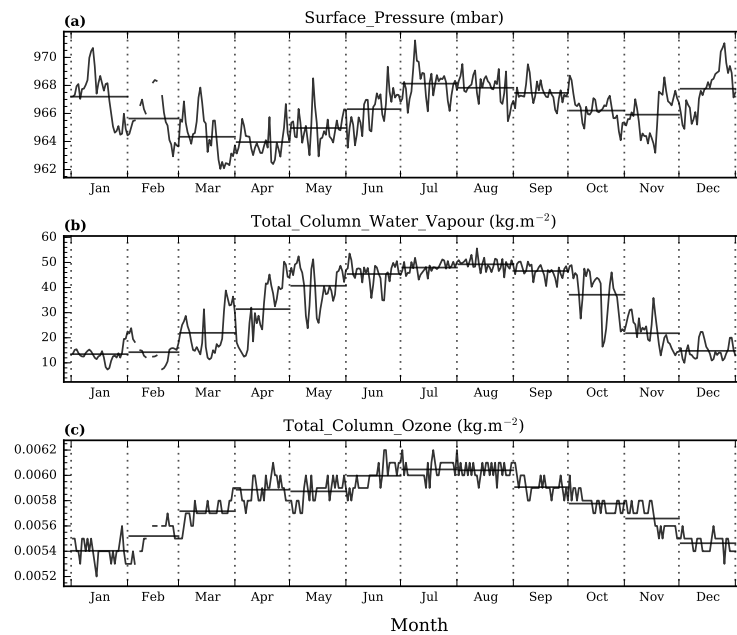
Figure 3. (**a**) Surface pressure, (**b**) total column water vapor, and (**c**) total column ozone variations in Maroua in 2014, extracted from European Center for Medium-Range Weather Forecasts (ECMWF) databases. Horizontal segments represent monthly averages and vertical dashed lines represent month delimitations.

The TCO annual average was 5.8×10^{-3} kg/m^2; its variation resembled a parabolic curve with a minimum of around 5.4×10^{-3} kg/m^2 and a maximum of around 6.0×10^{-3} kg/m^2. The ozone concentration followed the TCWV seasonal variations; thus the minimum occurred during the dry season, while the maximum occurred during the wet season. These variations are usual and were similar to those in N'djamena (12.12° N, 14.92° E), a neighboring area, where, although the high insolation dry period appears to be favorable for an abundant ozone production, the contrary occurs for the TCO variation, which is driven by wind dynamics over West Africa [48]. The same type of evolution is also observed in tropical Indian regions (latitudes <20° N), where TCO concentration raise and the peak has been related to the monsoon occurrence [49].

3.2.2. Total Cloud Cover

Clouds are great obstacles for solar radiation reaching the earth's surface because of the well-known parasol effect, which contributes to the thermal regulation of the earth [50,51]. Figure 4a presents the temporal distribution of the ECMWF TCC over Maroua at 12:00 UTC in 2014, while the TCC frequency histogram is represented in Figure 4b with bin widths of 0.05. January had the lowest TCC monthly average (around 0.2), while the maximum value was found in August (around 0.7), corresponding to the maximum of the TCWV. The annual average was about 0.45. During the dry season, the TCC decreased from October to January and then increased until April. The monsoon onset corresponded here to a TCC decrease and was followed by a peak in August with a small spacing period of cloud occurrence. During the other months and particularly in the dry season, the TCC peaks were more distant, meaning that there was a clear sky more often. In Figure 4b, the probability to have a cloudless scene (TCC ≤ 0.05) during the year was weak, about 16%. For an overcast sky, this probability fell to 9%, certainly as a result of the short rainy season. Apart from these two cases, clouds are constantly present in Maroua's atmosphere, and each cloud fraction (in the range [0–1]) can equitably occur with a probability of around 4%. The simulation of radiances for a cloudy scene requires the insertion of cloud parameters into the RTC. As these were not available for this first study, the DGSR comparison and statistical analysis were particularly focused on cloudless scenes identified in the first bin. It is

nevertheless important to plan the retrieval of cloud properties in order to better characterize the atmosphere and then simulate DGSR for these most recurrent scenes.
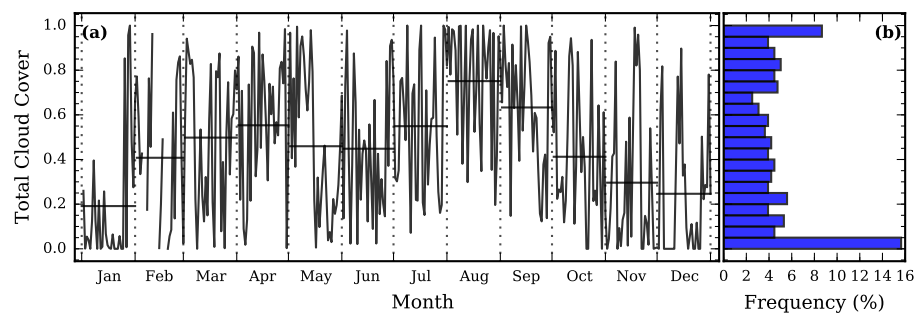

Figure 4. (**a**) European Center for Medium-Range Weather Forecasts (ECMWF) 12 UTC total cloud cover (TCC) variation and (**b**) its frequency histogram in Maroua in 2014. Horizontal segments represent TCC monthly averages, and vertical dashed lines represent month delimitations.

3.2.3. Vertically Distributed Quantities

In addition to total column quantities, vertical profiles give information on the structure of the atmosphere and can also be inserted into MODTRAN. We thus extracted the vertical profiles of the temperature, pressure, humidity and horizontal wind components. We present these profiles in Figure 5 in term of anomalies, which are the deviation of a parameter to its annual mean, at each altitude level.

In Figure 5a, atmospheric pressure anomalies are more marked in the first kilometers of the troposphere than in the upper levels. From the end of February to the beginning of June, deep in the dry season, the hot surface warmed up the air, resulting in its convection and a depression area in the first kilometers of the atmosphere. The same depression phenomenon occurred from mid-October to -November. The rest of the year, there were high pressure conditions, particularly during August and September in the rainy season. The pressure profiles were clearly linked to the temperature profile evolution during 2014 (Figure 5b). Two warmer periods clearly appeared, one from the end of February to the beginning of June, and the other from mid-October to -November. The coolest period occurred from July to September during the rainy season. Some cold periods also appeared in December, January and February that induced a corresponding pressure rise. In Figure 5c, we can observe that in the first 10 km, the relative humidity logically followed the seasonal variations, with low humidity and high humidity during the dry and monsoon seasons respectively. The relative humidity variations presented similarities with the temporal series of the water vapour content registered in Niamey in 2006 [11]. Regarding the components of horizontal wind in the low troposphere (Figure 5d,e), U is the zonal wind westerly oriented, and V is the meridional wind southerly oriented.

Two circulation regimes appear clearly: during the dry season, in the first 2 km of the atmosphere, the zonal and the meridional wind component anomalies were negative, meaning that the wind blew from the north, corresponding to the Harmattan wind. During the wet season (June–September), both wind component directions were reversed (positive U and V anomalies) with the monsoon wind coming from the south. The "false onset" of the monsoon occurred here between mid-April and -May, considering the first arrival of the ITF in Maroua and its rapid retirement before the "true onset" of the monsoon on May 20. This is also visible through the corresponding TCWV and relative humidity peaks (see Figures 3b and 5c, respectively), which rose and remained high until October 7. In the mid- and upper-troposphere, during the dry season, the subtropical westerly jet (STJ) blew. With the arrival of the monsoon flux during the wet season, it was shifted northward (negative anomaly of U wind) and was replaced in the mid-troposphere by the AEJ between May and October, as noticed in Niamey in 2006 [11]. These phenomena, previously detected in Niamey in 2006 and largely explained in [9], presented in Maroua a temporal shift of about 2 weeks. This delay could be due to the 12 year

difference between the two databases used. However, further investigations are necessary, knowing that the determination of the effective start of the rainy season is capital for sowing in such regions.
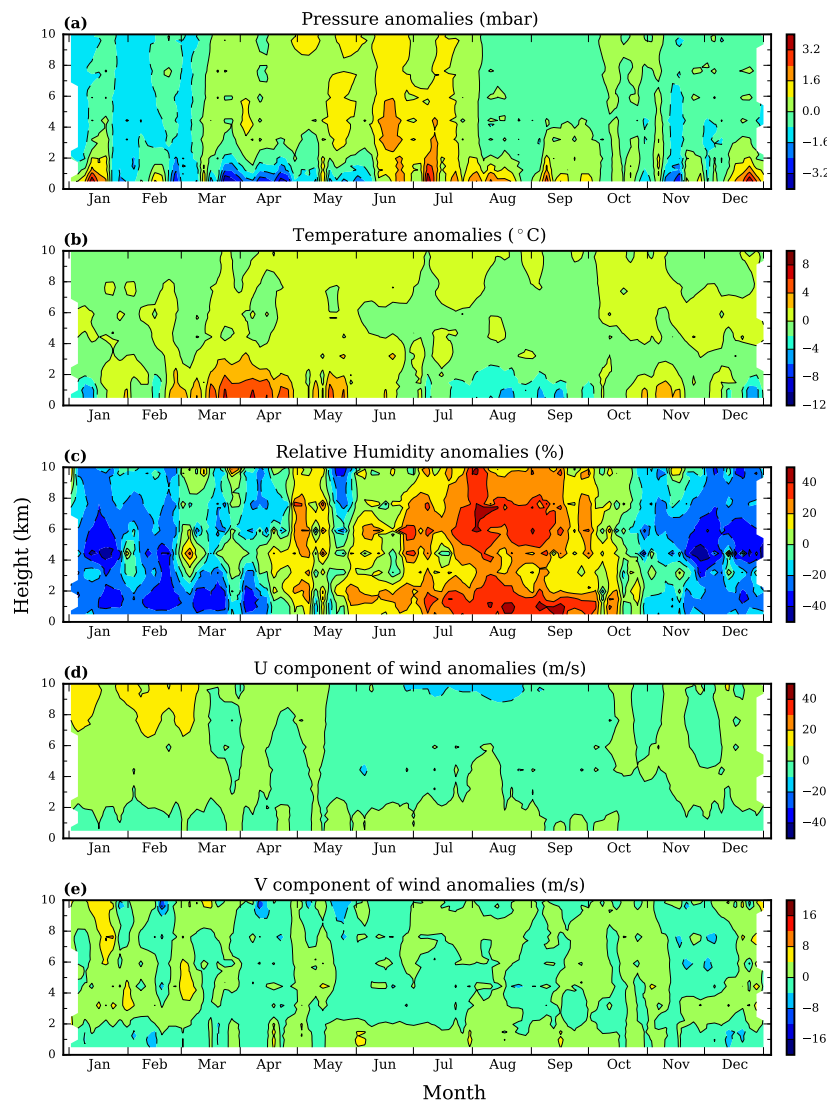

Figure 5. Differences between the mean of atmospheric vertical parameters extracted from European Center for Medium-Range Weather Forecasts (ECMWF) databases and (**a**) pressure, (**b**) temperature, (**c**) relative humidity, (**d**) U component of wind and (**e**) V component of wind in Maroua in 2014.

The analysis of the ECMWF atmospheric profiles shows that the Maroua atmosphere state and dynamics present many similarities with what was reported in some studies in West Africa, a neighboring zone [9,11,47,48]. Adding to this, the good correlation coefficients obtained between ECMWF and measured meteorological data at ground level show the capacity of ECMWF profiles to characterize the Maroua atmosphere and therefore show the possibility to use these in solar radiation simulation.

3.3. Setting and Computation of DGSR in Maroua

The most basic way to compute DGSR in Maroua with MODTRAN RTC is as specified in Section 2.3, using the tropical standard atmosphere. Clear-sky DGSR was simulated for the six aerosol models specified in Table 1. Maroua is mostly a semi-arid area, and in the absence of in situ spectral data, the surface albedo was set to the common value for the desert albedo of 0.3. Full

range (cloudless and cloudy) in situ measurements are represented in Figure 6a together with all clear-sky DGSR simulated. Data from January to August are the averages of DGSR simulated at 12:00, 12:15 and 12:30 UTC in order to correspond to the 30 min averaged measurements during this period. Starting in August, the measurement frequency was increased to 5 and 1 min averages. These measured data were thus directly compared to 12:00 UTC simulations. All the simulated DGSR curves have practically the same shape, mainly following the seasonal variations of the global solar radiation measured during the year. The DGSR curves simulated are very smooth, with standard profiles. Indeed, no specific information on daily atmospheric parameter variations is inserted, and the databases used here comprised only parameter values averaged over long time periods. Maroua ECMWF atmospheric profiles completed with standard values for missing data were used to refine the simulations. To evaluate the impact of the use of these profiles, we computed the clear-sky DGSR in this case with the six previous aerosol models and compared these again with the same in situ measurements (Figure 6b). In addition to the seasonal variations, we observed more variability of the DGSR, which appeared to be sensitive to the ECMWF profiles. The better representation of the daily variation of humidity modified the DGSR in this case. Compared to the simulations, measured DGSRs clearly presented many variations, as a result of cloud cover and rain, particularly during the rainy season or when aerosol loading was large. Concerning the six aerosol models, for both the standard and ECMWF profiles, the simulations were close to measurements in the following order: IHAZE = 0, 10, 1, 5bis, 2 and 5. However, we note that the simulated DGSR was smaller than the measured value for any aerosol model, while we expected the contrary at least for the case IHAZE = 0 (no cloud and no aerosols). We have not yet been able to clarify this situation, even with the adjustments of the DGSR simulation settings. Given that the ECMWF profiles presented good correlation coefficients compared to observations, this bias was likely due to dust on the solar radiation sensor or calibration issues. An alternative to overcome this difficulty would be to compare observations and the simulated DSGR with other sources of surface radiative fluxes, such as CERES SYN1deg-3HOUR retrievals (https://ceres.larc.nasa.gov/products.php?product=SYN1deg) or the ECMWF forecast product. This will be considered in future work. Keeping in mind this problem, in the following, we focus on the improvements as a result of the use of the ECMWF profiles and aerosol models, not in terms of absolute values but in terms of correlations.
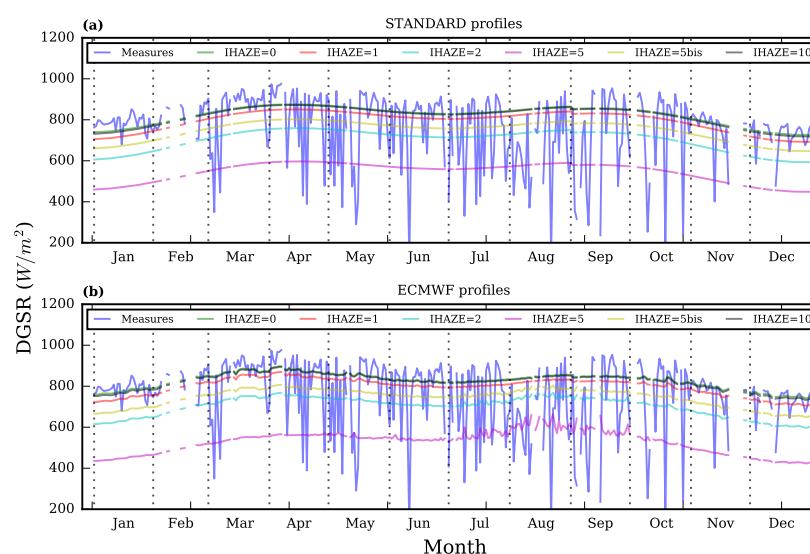

Figure 6. Representation of clear-sky downward global solar radiation (DGSR) simulated with (**a**) a standard atmosphere and (**b**) the insertion of European Center for Medium-Range Weather Forecasts (ECMWF) atmospheric profiles in Maroua in 2014. Simulations were done for six moderate-resolution transmittance (MODTRAN) default aerosol models. Corresponding DGSR measured is also represented for both cloudless and cloudy days. Vertical dashed lines represent month delimitations.

To find statistics and to examine more rigorously the suitability of aerosols models, we removed cloudy scenes visible in Figure 6 (blue line asperities) by establishing on DGSR data a cloud mask setting (TCC < 0.05) to select clear-sky conditions. Statistics performed on these data are presented in Table 3 for each aerosol model and for the standard and ECMWF profiles. R is the correlation coefficient. The RMSE, MBE and mean absolute error (MAE) are expressed in terms of relative values [52], as we now focus on data dispersion rather than on absolute values. Regarding the correlation values in Table 3, we see that independently of the chosen case, R was greater than 0.75 and was not specifically influenced by an aerosol type. Inserting the ECMWF atmospheric profiles slightly improved the correlation for each aerosol model, except for IHAZE = 5 (urban aerosol model), for which this slightly deteriorated. Errors were lower as a result of the use of the ECMWF atmospheric profile, except for IHAZE = 5, for which they increased. Inserting the ECMWF profiles improved the simulations, as the MODTRAN RTC considers the effect of the ECMWF humidity variation on aerosol properties as a result of the induced water vapor condensation onto aerosol particles. The aerosol size is therefore increased and their radiative properties modified [30]. Despite the bias existing between the simulated and measured DGSR, we observed that for both the standard and ECMWF atmospheric profiles, the DGSR was slightly underestimated for IHAZE = 0, 10; a little more underestimated for IHAZE = 1, 2, 5bis; and highly underestimated for IHAZE = 5 (see also Figure 6a,b). Two groups of aerosols appeared: the first induced high errors (IHAZE = 2, 5), and the second induced slight errors (IHAZE = 0, 1, 5bis, 10). These two groups corresponded to visibility: (1) rural and urban aerosol models with a low visibility (5 km) for IHAZE = 2, 5; and (2) models with very high visibility (no aerosols), high visibility (rural and urban aerosol of 23 km visibility) and with a variable visibility set by wind speed (desert aerosol).

Table 3. Correlation coefficient (R) and statistical error comparisons between measured and simulated clear-sky downward global solar radiation (DGSR) for six moderate-resolution transmittance (MODTRAN) default aerosol models. Simulations were done with a standard atmosphere and with the insertion of European Center for Medium-Range Weather Forecasts (ECMWF) atmospheric profiles in Maroua in 2014. Root-mean-squared error (RMSE), mean bias error (MBE) and mean absolute error (MAE) are relative values in percent.

		Standard Profiles				ECMWF Profiles		
IHAZE	**R**	**RMSE (%)**	**MBE (%)**	**MAE (%)**	**R**	**RMSE (%)**	**MBE (%)**	**MAE (%)**
0	0.781	6.430	−3.682	5.170	0.819	5.308	−1.460	3.931
1	0.778	9.158	−7.499	8.364	0.814	7.541	−5.627	6.629
2	0.772	20.182	−19.475	19.731	0.802	19.331	−18.660	18.865
5bis	0.776	14.200	−13.183	13.646	0.804	13.768	−12.781	13.187
5	0.768	38.507	−38.131	38.131	0.766	41.633	−41.275	41.275
10	0.779	6.891	−4.456	5.754	0.817	5.544	−2.290	4.326

The case IHAZE = 0 (no aerosol) had the best statistics. This was an ideal case because the atmosphere cannot be absolutely free of aerosols, particularly in the Sahelian region, where rain is not recurrent. This case should give DGSR values higher than the measured values, but we observed that measurements were higher than for all the simulated cases. For rural and urban aerosol models, compared to the case with no aerosol, the correlation deteriorated at the same time as the visibility decreased going from IHAZE of 1 to 2 and from IHAZE of 5 to 5bis. In MODTRAN, the visibility is related to the extinction coefficient (EXT) according to the Koschmieder formula as VIS = 3.912/EXT [41]. A visibility of 23 km corresponds to an extinction of 0.17 km^{-1}; thus for the 2 km boundary layer height, it gives an aerosol optical depth (AOD) of 0.34. When the visibility fells to 5 km, the AOD becomes 1.56, which is a relatively high value. The most realistic case for this site, owing to R, RMSE and MBE values, was the case IHAZE = 10 for the desert aerosol model, which was logical for this Sahelian site type and had the advantage of setting the visibility as a function of the

wind speed, as opposed to the fixed visibility aerosol models. It worked better in association with ECMWF atmospheric profiles that contained wind parameters, even if the correlation between the measurements and ECMWF wind surface data was not perfect (see Figure 2). It would be interesting to study aerosol properties and dynamics in this area and compare the model's AOD to those effectively measured or evaluated: this would give better selection criteria for the default aerosol model. In [53], the importance of the aerosol composition in estimating incoming solar radiation is demonstrated for Dakar and Niamey (West Africa) with comparable climate conditions. Thus, aerosols could be better accounted for in future works with the adjustments of AOD values in the simulations, using satellite or monitoring atmospheric composition and climate (MACC) data [54], thus ameliorating DGSR estimations. Additionally, surface albedo was fixed to the planetary value 0.3 because of missing information. Some studies [55,56] reveal that this parameter should be carefully designed in climate models. In fact, surface albedo varies during the year, particularly in the rainy season when vegetation arises in this sahelian zone [57]. The study of aerosol properties and surface albedo variation in Maroua will be considered in further works.

To refine our comparisons and because the measurement sampling was modified in August, we present the previous statistics in Table 4 only for the MODTRAN desert aerosol model under cloudless conditions and for the two periods (January–May and October–December) in the dry season. During the rainy season, there was no day with cloudless conditions at 12:00 UTC, and cloud microphysical parameters were not available for this study. The correlation and the errors were much better in the second dry period, after the rainy season. Differences arose certainly with the change in measurement sampling, as DGSR values were averaged during the first dry period over a 30 min period, while in the second dry period it was instantaneous values that were used. Another reason may be that the rain had cleaned the sensor surfaces, which were likely dusty in the first dry period. The absence of cloudless scenes during the rainy season leads us to conclude that efforts have to be made in order to assess cloud microphysics to enlarge the number and produce more reliable DGSR data.

Considering only cloudless scenes rather than all the dynamical conditions in Maroua somewhat restricts the conclusions of the study. Clear-sky irradiation of the measured data could have been generated using the Long and Ackerman method [58] and compared with clear-sky irradiation simulated with MODTRAN in the presence of ECMWF atmospheric profiles. This approach would have produced clear-sky solar data for cloudy scenes, to compare their corresponding cloudless MODTRAN simulations with ECMWF atmospheric profiles. Thus, together with the comparison under clear conditions, the performance of our method under all atmospheric conditions would have been evaluated. Unfortunately, the absence of measured diffuse irradiation necessary for the method of clear-sky irradiation generation made this impossible. The difficulty faced here is another argument to restart both global and diffuse solar radiation measurements in this region.

Table 4. Correlation coefficient (R) and statistical error comparison between measured and simulated clear-sky downward global solar radiation (DGSR) for two dry season periods (January–May and October–December), with the insertion of European Center for Medium-Range Weather Forecasts (ECMWF) atmospheric profiles, in Maroua in 2014. IHAZE = 10. Root-mean-squared error (RMSE), mean bias error (MBE) and mean absolute error (MAE) are relative values in percent.

	R	RMSE (%)	MBE (%)	MAE (%)
Dry period 1	0.759	6.702	−3.263	5.604
Dry period 2	0.909	2.610	−0.756	2.314

4. Summary and Perspectives

In this work, ECMWF atmospheric profiles have been used to characterize ground-level and vertical atmospheric profiles in the site of Maroua, where in situ measurements are very scarce. A set of 12:00 UTC daily atmospheric data of this site was extracted for the year 2014 and was

used to simulate DGSR. Over the same period, a campaign was carried out to measure the pressure, temperature, humidity, wind speed and global solar radiation at ground level. A comparison of ECMWF atmospheric parameters with surface measurements has shown good correlation coefficients and slight errors for pressure, temperature and humidity, whereas some discrepancies have been observed for wind speed, making the ECMWF wind speed for this site to be used with caution. For upper atmospheric levels, there was unfortunately no in situ measurement to compare with the ECMWF data acquired to improve the characterization of the site atmosphere. However, the ECMWF profiles showed variations close to what was observed in the West African region, particularly in Niamey, Niger, with a Maroua meteorological variability driven by the biseasonal mode with a monsoon flux. A delay of the monsoon true onset was observed in Maroua in comparison with Niamey, Niger and needs to be investigated to ameliorate a prediction of the start of the rainy season. The annual variation and magnitude of the TCO concentration were similar to those recorded in N'djamena, and the peak occurred during the monsoon, as in Indian tropical regions. DGSR was then simulated with MODTRAN RTC under two conditions: (1) with standard tropical atmosphere, and (2) with ECMWF atmospheric profiles. The ECMWF TCC was used to choose cloudless days and find statistics on solar radiation data. Compared to the simulation in standard atmosphere, the ECMWF atmospheric profiles improved the correlation coefficient and reduced the errors, even in the presence of aerosols. Simulations done with MODTRAN aerosols were sensitive to humidity, which was better expressed along with other atmospheric components in ECMWF atmospheric profiles than in standard profiles. This demonstrates that in the absence of in situ measurements, ECMWF atmospheric profiles can well characterize the site at all altitudes. Notwithstanding the constant bias observed between simulations and measurements, and likely as a result of calibration issues or dust on the sensor, these are also suitable for computing and estimating solar radiation in its various components at this site.

Everyone should be involved in the fight against climate change; particularly, developing countries should take an active part in all stages of the process. Thus, some efforts have to be made in order to improve local capabilities in the monitoring of climate change technologies and to ameliorate responses to emergencies. The case of Maroua in Cameroon is a perfect illustration of this situation, and the present work is an overview of the processes to overcome it. This study is a first step to show the possibility to use ECMWF atmospheric profiles in the characterization of the atmosphere state and dynamics, when no in situ data are available or to complete existing data in Maroua. It also presents an overview of efforts and improvements that still need to be made in order to reproduce the measurements of ground-based meteorological data. Some remaining aspects to investigate in order to achieve the previous goals are enlightened:

- In order to maintain a good data accuracy, calibration settings or cleaning must be performed on solar radiation and wind sensors, and the lowest temporal resolution must be used in measuring.
- Wind data biases have to be investigated further in order to determine any source of inaccuracy. A three-party comparison between ECMWF, measured, and MERRA or CFS wind data is considered.
- Surface albedo variations, aerosol optical properties and cloud microphysics parameters could be assessed with the use of satellite data retrievals (ECMWF, MACC, MERRA,... models) and could thus better characterize the atmosphere.
- Another issue relates mainly to solar radiation simulation, which may gain accuracy with the insertion of aerosol properties and surface albedo variations, and which could be more reliable with the consideration of cloud parameters to simulate DGSR under any atmospheric conditions. Validations may be performed by comparing these to CERES or ECMWF surface radiative flux products.

The use of ECMWF atmospheric profiles responds to the important lack of meteorological data and also gives access, through simulation, to diffuse, direct and global solar radiation components that was no longer accessible at this site. Because this problem is not specific to the region of Maroua,

the achievement of the present work will be helpful in other sites where in situ measurements are also scarce.

Author Contributions: Donatien Njomo and Philippe Dubuisson conceived the research and provided logistics and technical guidance. Céline Cornet and Leonard Akana Nguimdo analyzed the work and commented the results and figures. Cyrille Fotsing Talla collected data, made the computations, applied the analysis methods and wrote the manuscript.

Conflicts of Interest: The authors declare no conflict of interest.

References

1. Le-Treut, H.; Somerville, R.; Cubasch, U.; Ding, Y.; Mauritzen, C.; Mokssit, A.; Peterson, T.; Prather, M. Historical Overview of Climate Change. In *Climate Change 2007: The Physical Science Basis. Contribution of Working Group I to the Fourth Assessment Report of the Intergovernmental Panel on Climate Change*; Cambridge University Press: Cambridge, UK, 2007.

2. Forster, P.; Ramaswamy, V.; Artaxo, P.; Berntsen, T.; Betts, R.; Fahey, D.W.; Haywood, J.; Lean, J.; Lowe, D.C.; Myhre, G.; et al. Changes in Atmospheric Constituents and in Radiative Forcing. In *Climate Change 2007: The Physical Science Basis. Contribution of Working Group I to the Fourth Assessment Report of the Intergovernmental Panel on Climate Change*; Cambridge University Press: Cambridge, UK, 2007.

3. Trenberth, K.E.; Jones, P.D.; Ambenje, P.; Bojariu, R.; Easterling, D.; Tank, A.K.; Parker, D.; Rahimzadeh, F.; Renwick, J.A.; Soden, B.; et al. Observations: Surface and Atmospheric Climate Change. In *Climate Change 2007: The Physical Science Basis. Contribution of Working Group I to the Fourth Assessment Report of the Intergovernmental Panel on Climate Change*; Cambridge University Press: Cambridge, UK, 2007.

4. Fotsing, T.C.; Njomo, D.; Cornet, C.; Dubuisson, P.; Nsouandele, J.L. Acquisition and study of global solar radiation in Maroua-Cameroon. *Int. J. Renew. Energy Res.* **2015**, *5*, 910–918.

5. Abossolo, S.A.; Amougou, J.A.; Tchindjang, M. *Perturbation Climatiques et Pratiques Agricoles Dans les Zones Agroécologiques du Cameroun: Changements Socio-économiques et Problématiques d'adaptation Aux Bouleversements Climatiques*; Connaissances et Savoirs: Saint-Denis, France, 2017.

6. Molua, E. Climatic trends in Cameroon: Implications for agricultural management. *Clim. Res.* **2006**, *30*, 255–262.

7. Molua, E. Turning up the heat on African agriculture: The impact of climate change on Cameroon's agriculture. *Afr. J. Agric. Resour. Econ.* **2008**, *2*, 45–64.

8. Redelsperger, J.-L.; Thorncroft, C.D.; Diedhiou, A.; Lebel, T.; Parker, D.J.; Polcher, J. African monsoon multidisciplinary analysis: An International Research Project and Field Campaign. *Bull. Am. Meteorol. Soc.* **2006**, *87*, 1739–1746.

9. Slingo, A.; Bharmal, N.A.; Robinson, G.J.; Settle, J.J.; Allan, R.P.; White, H.E.; Lamb, P.J.; Lélvé, M.I.; Turner, D.D.; McFarlane, S.; et al. Overview of observations from the RADAGAST experiment in Niamey, Niger: Meteorology and thermodynamic variables. *J. Geophys. Res. Atmos.* **2008**, *113*, D00E01.

10. Janicot, S.; Redelsperger, J.-L.; Lebel, T. La mousson ouest-africaine: Introduction à quelques contributions du programme d'étude multidisciplinaire AMMA. *La Météorologie* **2012**, doi:10.4267/2042/48125.

11. Louf, V.; Pujol, O.; Sauvageot, H.; Riédi, J. Seasonal and diurnal water vapour distribution in the Sahelian area from microwave radiometric profiling observations. *Q. J. R. Meteorol. Soc.* **2015**, *141*, 2643–2653.

12. Akana, N.L.; Njomo, D. Assessing the aerosol optical thickness in Cameroon using ground-based solar radiation measurements. *Adv. Sci. Lett.* **2010**, *3*, 1–7.

13. Akana, N.L.; Njomo, D. Profiles of cloud fraction and water content deduced from ground-based solar radiation measurements. *Asian-Pac. J. Atmos. Sci.* **2010**, *46*, 483–496.

14. Oumbe, A.; Wald, L.; Blanc, P.; Schroedter-Homscheidt, M. Exploitation of radiative transfer model for assessing solar radiation: The relative importance of atmospheric constituents. In Proceedings of the

1st International Congress on Heating, Cooling and Buildings (EUROSUN 2008), Lisbonne, Portugal, 7–10 October 2008; ISES: Freiburg, Germany, 2008; p. 403.

15. Bernlöhr, K. Impact of atmospheric parameters on the atmospheric Cherenkov technique. *Astropart. Phys.* **2000**, *12*, 255–268.

16. Noh, Y.-C.; Sohn, B.-J.; Kim, Y.; Joo, S.; Bell, W. Evaluation of Temperature and Humidity Profiles of Unified Model and ECMWF Analyses Using GRUAN Radiosonde Observations. *Atmosphere* **2016**, *7*, 94.

17. Calbet, X.; Schlüssel, P.; Hultberg, T.; Phillips, P.; August, T. Validation of the operational IASI level 2 processor using AIRS and ECMWF data. *Adv. Space Res.* **2006**, *37*, 2299–2305.

18. Martinez, M.A.; Mercedes, V. Validation of SAFNWC Layer Precipitable Water Using ECMWF Analysis Profile and Radiosonde. Available online: https://www.eumetsat.int/cs/idcplg?IdcService=GET_FILE& dDocName=pdf_conf_p48_s6_16_martinez_p&allowInterrupt=1&noSaveAs=1&RevisionSelectionMethod= LatestReleased (accessed on 11 June 2017).

19. Gobiet, A.; Foelsche, U.; Steiner, A.K.; Borsche, M.; Kirchengast, G.; Wickert, J. Climatological validation of stratospheric temperatures in ECMWF operational analyses with CHAMP radio occultation data. *Geophys. Res. Lett.* **2005**, *32*, L12806.1–L12806.5.

20. Njomo, D. Les solutions solaires aux besoins énergétiques prioritaires des populations rurales des pays en développement. *Revue de l'énergie* **1988**, *404*, 498–503.

21. Njomo, D. Modélisation des variations mensuelles de l'irradiation solaire reçue au Cameroun. In *Modeling, Simulation and Control*; AMSE Press: Oak Ridge, TN, USA, **1989**, Volume 18, pp. 39–64.

22. Boukerzaza, N.; Chaker, A.; Haddad, Z. Influence de l'irradiation globale sur les caractéristiques de fonctionnement d'un distillateur solaire. In *Revue des Energies Renouvelables ICRESD-07 Tlemcen*; CDER: Alger, Algerie, 2007; pp. 229–234.

23. Kilic, B. Evaluating of Renewable Energy Potential in Turkey. *Int. J. Renew. Energy Res.* **2011**, *1*, 259–264.

24. Mejdoul, R.; Taqi, M. The mean hourly global radiation prediction models investigation in two different climate regions in Morocco. *Int. J. Renew. Energy Res.* **2012**, *2*, 608–617.

25. Rigollier, C.; Lefèvre, M.; Wald, L. The method heliosat-2 for deriving shortwave solar radiation from satellite images. *Sol. Energy* **2004**, *77*, 159–169.

26. Njomo, D.; Wald, L. Solar irradiation retrieval in Cameroon from meteosat satellite imagery using the heliosat_2 method. *ISESCO Sci. Technol. Vis.* **2006**, *2*, 19–24.

27. Oumbe, A.; Blanc, P.; Ranchin, T.; Schroedter-Homscheidt, M.; Wald, L. A new method for estimating solar energy resource. In Proceedings of the 33rd International Symposium on Remote Sensing of Environment (ISRSE), Stresa, Italy, 4–8 May 2009; Joint Research Center: Ispra, Italy, 2009; p. 773.

28. Oumbe, A.; Wald, L. A parameterisation of vertical profile of solar irradiance for correcting solar fluxes for changes in terrain elevation. In Proceedings of the Earth Observation and Water Cycle Science Conference, Frascati, Italy, 18–20 November 2009; ESA: Paris, France, 2010; p. S05.

29. Akana, N.L.; Njomo, D. Spatial and temporal distributions of downwelling solar radiation in Cameroon as derived using a parameterized solar radiative transfer model in a molecular atmosphere. *JP J. Heat Mass Transf.* **2009**, *3*, 73–93.

30. Gurlit, W.; Bösch, H.; Bovensmann, H.; Burrows, J.P.; Butz, A.; Camy-Peyret, C.; Dorf, M.; Gerilowski, K.; Lindner, A.; Noël, S.; et al. The UV-A and visible solar irradiance spectrum: Inter-comparison of absolutely calibrated, spectrally medium resolution solar irradiance spectra from balloon- and satellite-borne measurements. *Atmos. Chem. Phys.* **2005**, *5*, 1879–1890.

31. Viúdez-Mora, A.; Calbó, J.; González, J.A.; Jiménez, M.A. Modeling atmospheric longwave radiation at the surface under cloudless skies. *J. Geophys. Res.* **2009**, *114*, doi:10.1029/2009JD011885.

32. Viúdez-Mora, A. Atmospheric Downwelling Longwave Radiation at the Surface during Cloudless and Overcast Conditions. Ph.D. Thesis, Universitat de Girona, Girona, Spain, 2011.

33. Hulley, G.; Hook, S. *Hyspiri Level-2 Tir Surface Radiance Algorithm Theoretical Basis Documen*; Technical Report; Jet Propulsion Laboratory; California Institute of Technology: Pasadena, California, 2001. Available online: https://hyspiri.jpl.nasa.gov/downloads/Algorithm_Theoretical_Basis/HyspIRI_L2_ Surface_Radiance_JPL_Pub_11-1.pdf (accessed on 11 June 2017).

34. Schulze, S. A Comparison of MODTRAN and Rttov Radiative Transfer Models for Lake Surface Water Temperature Retrieval. Master's Thesis, Institute of Geography and Oeschger Centre for Climate Change Research, University of Bern, Bern, Switzerland, 2012.

35. Chiacchio, M.; Solmon, F.; Giorgi, F.; Stackhouse, P., Jr.; Wild, M. Evaluation of the radiation budget with a regional climate model over Europe and inspection of dimming and brightening. *J. Geophys. Res. Atmos.* **2015**, *120*, 1951–1971.

36. Alexandri, G.; Georgoulias, A.K.; Zanis, P.; Katragkou, E.; Tsikerdekis, A.; Kourtidis, K.; Meleti, C. On the ability of RegCM4 regional climate model to simulate surface solar radiation patterns over Europe: An assessment using satellite-based observations. *Atmos. Chem. Phys.* **2015**, *15*, 13195–13216.

37. ECMWF/WCRP Level III-A Global Atmospheric Data Archive, The Description of the Evolution of the ECMWF Forecasting System and Corresponding Archive; Technical Report; 1999; p. 126. Available online: https://rda.ucar.edu/datasets/ds115.3/docs/evolution.pdf (accessed on 11 June 2017).

38. Persson, A. *User Guide to ECMWF Forecast Products*, Version 1.2; ECMWF: Shinfield, Reading, UK, 2015. Available online: https://www.ecmwf.int/sites/default/files/User_Guide_V1.2_20151123.pdf (accessed on 11 June 2017).

39. DAVIS. Wireless Vantage Pro2^{TM} & Vantage Pro2^{TM} Plus Stations. Available online: https://www.davisnet.com/product_documents/weather/spec_sheets/6152_62_53_63_SS.pdf (accessed on 11 June 2017).

40. Berk, A.; Anderson, G.P.; Acharya, P.K.; Chetwynd, J.H.; Bernstein, L.S.; Shettle, E.P.; Matthew, M.W.; Golden, S.M. MODTRAN4 User's Manual. 2003. Available online: http://www.cis.rit.edu/~cnspci/references/berk2003.pdf (accessed on 11 June 2017).

41. Abreu, L.W.; Anderson, G.P. (Eds.) The MODTRAN 2/3 Report and Lowtran 7 Model. 1996. Available online: http://web.gps.caltech.edu/~vijay/pdf/modrept.pdf (accessed on 11 June 2017).

42. Rothman, L.S.; Gamache, R.R.; Tipping, R.H.; Rinsland, C.P.; Smith, M.A.H.; Benner, D.C.; Devi, V.M.; Flaud, J.-M.; Camy-Peyret, C.; Perrin, A.; et al. The HITRAN molecular database. *J. Quant. Spectrosc. Radiat. Transf.* **1992**, *48*, 469–507.

43. Rothman, L.S.; Rinsland, C.P.; Goldman, A.; Massie, S.T.; Edwards, D.P.; Flaud, J.-M.; Perrin, A.; Dana, V.; Mandin, J.-Y.; Schroeder, J.; et al. The HITRAN molecular spectroscopic database and hawks (HITRAN atmospheric workstation): 1996 edition. *J. Quant. Spectrosc. Radiat. Transf.* **1998**, *60*, 665–710.

44. Sandu, I.; Beljaars, A.; Bechtold, P.; Mauritsen, T.; Balsamo, G. Why is it so difficult to represent stably stratified conditions in numerical weather prediction (NWP) models? *J. Adv. Model. Earth Syst.* **2013**, *5*, 117–133.

45. Holtslag, A.A.M.; Svensson, G.; Baas, P.; Basu, S.; Beare, B.; Beljaars, A.C.M.; Bosveld, F.C.; Cuxart, J.; Lindvall, J.; Steeneveld, G.J.; et al. Stable Atmospheric Boundary Layers and Diurnal Cycles: Challenges for Weather and Climate Models. *Bull. Am. Meteor. Soc.* **2013**, *94*, 1691–1706.

46. Liu, Z.; Schweiger, A.; Lindsay, R. Observations and Modeling of Atmospheric Profiles in the Arctic Seasonal Ice Zone. *Mon. Weather Rev.* **2015**, *143*, 39–53.

47. Thorncroft, C.D.; Nguyen H.; Zhang, C.; Peyrillé, P. Annual cycle of the West African monsoon: Regional circulations and associated water vapour transport. *Q. J. R. Meteorol. Soc.* **2011**, *137*, 129–147.

48. Oluleye, A.; Chilekwu, O.E. Analysis of temporal and spatial variability of total column ozone over West Africa using daily TOMS measurements. *Atmos. Pollut. Res.* **2013**, *4*, 387–397.

49. Madhu, V. Spatial and Temporal Variability of Total Column Ozone over the Indian Subcontinent: A Study Based on Nimbus-7 TOMS Satellite. *Atmos. Clim. Sci.* **2014**, *4*, 884–898.

50. Ardanuy, P.E.; Stowe, L.L.; Gruber, A.; Weiss, M. Shortwave, longwave, and net cloud-radiative forcing as determined from Nimbus 7 observations. *J. Geophys. Res.* **1991**, *98*, 18537–18549.

51. Gupta, S.K.; Staylor, F.W.; Darnell, W.L.; Wilber, A.C.; Ritchey, N.A. Seasonal variation of surface and atmospheric cloud radiative forcing over the globe derived from satellite data. *J. Geophys. Res.* **1993**, *98*, 20761–20778.

52. Hoff, T.E.; Kleissl, J.; Perez, R.; Renne, D.; Stein, J.S. Reporting of irradiance model relative errors. In Proceedings of the 2012 American Solar Energy Society Annual Conference (ASES), Denver, CO, USA, 13–17 May 2012.

53. Drame, M.S.; Ceamanos, X.; Roujean, J.L.; Boone, A.; Lafore, J.P.; Carrer, D.; Geoffroy, O. On the Importance of Aerosol Composition for Estimating Incoming Solar Radiation: Focus on the Western African Stations of Dakar and Niamey during the Dry Season. *Atmosphere* **2015**, *6*, 1608–1632.

54. Vermeulen, A.; Descloitres, J. *Final Description Document on SEVIRI Aerosol Product over Land*; ECMWF/MACCII: Reading, UK, 2014.

55. Oikarinen, L. Effect of surface albedo variations on UV-visible limb-scattering measurements of the atmosphere. *J. Geophys. Res.* **2002**, *107*, 4404.

56. He, T.; Liang, S.; Song, D.-X. Analysis of global land surface albedo climatology and spatial-temporal variation during 1981–2010 from multiple satellite products. *J. Geophys. Res. Atmos.* **2014**, *119*, 10281–10298.

57. Fondsdesol. Available online: http://newtec.univ-lille1.fr/fondsdesol/ (accessed on 11 June 2017).

58. Long, C.N.; Ackerman, T.P. Identification of clear skies from broadband pyranometer measurements and calculation of downwelling shortwave cloud effects. *J. Geophys. Res. Atmos.* **2000**, *105*, 15609–15626.